A Broadband Current Sensor based on the X-Hall Architecture

M. Crescentini, M. Biondi, R. Ramilli, P. A. Traverso,
G. P. Gibiino, A. Romani, M. Tartagni
DEI and ARCES
University of Bologna
Cesena, Italy
m.crescentini@unibo.it

M. Marchesi, R. Canegallo
Analog & Smart Power R&D
STMicroelectronics
Castelletto, Italy
marco.marchesi@st.com

***Abstract*— A broadband current sensor, which is fully integrated and galvanically-isolated, is presented in this paper. The current sensor relies only on a Hall-effect probe to realize the magnetic sensing core so as to minimize the cost and the occupied space. Bandwidth limitations of state-of-the-art Hall-effect probes are overcame by combining the novel X-Hall architecture with a wide bandwidth differential-difference current-feedback amplifier. A prototype implemented in 0.16-µm BCD technology demonstrates a bandwidth wider than 20 MHz. Offset, sensitivity and power consumption are comparable to the state of the art. This is the first Hall-only current sensor achieving a bandwidth higher than 3 MHz.**

Keywords*— *Current sensor, Hall sensor, XHall, Magnetic sensor, Bandwidth, CFA, DDA, CMOS, BCD, Offset reduction.

I. INTRODUCTION

Current sensors are crucial in many power circuits: they are used for feedback control, overcurrent detection (OCD) and other functionalities [1]. The modern trend in power electronics (e.g. automotive applications) is to move the switching rate of the power circuits to higher frequencies (up to the MHz range) so as to allow the shrinking of the passive components. As a consequence, there is a strong need for broadband current sensors which are small and, preferably, galvanically isolated from the power path. There exist different technological solutions for current measurements in power applications; they can be grouped as i) shunt-based sensors ii) coil-based magnetic sensors, and iii) Lorentz' magnetic sensors (e.g. Hall-effect). Table I summarizes and quickly compares the state of the art for all these sensor typologies. For each type of current sensor, the table highlights in red the challenges to be addressed so as to achieve all the specifications required by fast-switching power circuits. The high compatibility of Hall-effect sensors with standard CMOS processes allows the Hall-effect sensors to inherently achieve the targets of low-cost and reduced dimension, but the state-of-the-art bandwidth is not fully adequate since it is demonstrated up to 1 MHz [4]. A complete analysis of the dynamic effects in Hall-effect-based current sensors shows that the first limitation to the bandwidth is given by the spinning-current technique, which is the dynamic technique used to cancel the high intrinsic offset of the sensor, as well as the Flciker noise [5,6]. Therefore, to broaden the bandwidth up to tens of megahertzes, it is essential to eliminate the spinning-current technique and identify a static method able to reduce the high intrinsic offset of the sensor.

This work was supported by the ECSEL Joint Undertaking (JU) through EU H2020 program and Italy, Germany, The Netherlands, Spain, and Slovakia under Grant Agreement no. 737434.

TABLE I. OVERVIEW OF STATE-OF-THE-ART CURRENT SENSORS

Sensor Type	Bandwidth	DC measure	CMOS integration	Galvanic Isolation	Heat Dissipation	Occupied Space	Cost
SHUNT [2]	high	yes	**possible**	**no**	**yes**	**huge**	low
COIL [3]	very high	**no**	**hard**	yes	no	**huge**	**high**
HALL [4]	**limited**	yes	easy	yes	no	small	low

In this paper, a broadband current sensor relying only on the Hall-effect is presented. The sensor overcomes the bandwidth limitation of state-of-the-art Hall-effect sensors by combining the novel X-Hall DC biasing technique with a wide-bandwidth differential-difference current-feedback amplifier (DDCFA) (Fig. 1). The proposed sensor responds to all the requirements coming from fast-switching power circuits by offering a small, low-cost, and fast current sensor. The basic idea behind the X-Hall technique was presented, for the first time ever, at the 2018 IMEKO World Congress but only theoretical analysis and static measurements on the probe were reported [7]. In this paper, the X-Hall probe is combined with a dedicated readout circuit to realize a complete current sensor and dynamic performance are experimentally demonstrated.

A prototype of the proposed current sensor is implemented in 0.16-µm BCD technology. The magnetic field is generated by a current flowing through an on-chip copper strip and applies to the Hall-effect probe closed to it. The Hall voltage provided by the probe, to which a residual offset is superimposed, is then amplified by the broadband DDCFA. Preliminary measurements demonstrate an acquisition bandwidth of 20 MHz and show the potentiality to achieve even wider bandwidths. To our knowledge, this is the first Hall-only current sensor achieving a bandwidth higher than 3 MHz. Section II and Section III describes the X-Hall probe and the DDCFA, respectively. Section IV reports the experimental results, while Section V draws the final conclusions.

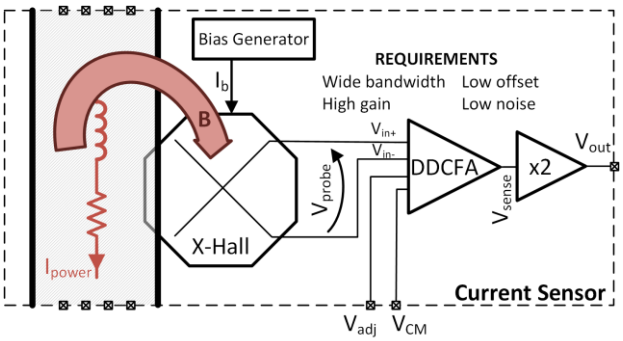

Fig. 1. Block scheme of the proposed broadband current sensor.

II. The X-Hall Sensor

The X-Hall consists of a novel sensor geometry combined with a DC biasing scheme that allow to get rid of the spinning-current technique and enlarge the acquisition bandwidth of the sensor up to the limit set by the capacitive load of the amplifier [5], [7].

The X-Hall probe consists of an octagonal, lowly-doped n-well contacted by 8 highly-doped contacts (Fig. 2-a) and surrounded by a p-well connected to ground. These contacts are grouped as bias contacts (B, T, L, R) and sense contacts (1, 2, 3, 4). Bias contacts are large sized to minimize the contact resistance while sense contacts are designed as small as possible to minimize the parasitic capacitance. Two nominally equal bias currents (I_A=I_B) are injected into the sensor through contacts T and B while contacts L and R are connected to ground. Bias contacts are oriented orthogonally to the edges of the n-well to realize the nominal current density distribution reported in Fig. 2-a. When a magnetic field B_z applies orthogonally to the plane identified by the octagonal n-well, then the current densities $J_A = J_{A,L} + J_{A,R}$ and $J_B = J_{B,L} + J_{B,R}$ unbalance on one side and the Hall voltage V_H appears on both the output voltages V_A and V_B with opposite signs and with superimposed offset voltages $V_{OS,A}$ and $V_{OS,B}$.

According to this biasing scheme, it is possible to consider the octagonal n-well region as two Hall-effect inner probes, probe A and probe B, with two separated output voltages: V_A and V_B. In the X-Hall architecture, the two voltages V_A and V_B are combined together by cross short-circuiting the sense contacts as shown in Fig. 2-b. The short circuits set the equality $V_A = -V_B = V_{probe}$ that minimizes the residual offset $V_{OS,H}$ on the output node (i.e. $V_{probe} = V_H + V_{OS,H}$). The resistive bridge model of the Hall probe (Fig. 3) helps to understand the effect of these short circuits on the offset. If we assume the same potential on the contacts B and T, then each resistance modelling a branch of the probe A is in parallel to a resistance modelling an opposite branch of the probe B in a common-centroid scheme. In this way, any offset generated by a global effect that creates a linear inhomogeneity (e.g. a resistivity gradient) is perfectly cancelled out. In a real device, the offset is generated by both global effects and local effects, and equality of the voltages on B and T terminal is not assured, thus, a small but non-zero residual offset $V_{OS,H}$ remains. To sum up, the X-Hall architecture provides a fair reduction of the intrinsic offset of the Hall-effect probe without requiring dynamic spinning of the bias current. In this way, the Hall-effect probe can be exploited up to the maximum achievable bandwidth set by the electronic readout circuit. Indeed, the bandwidth of the sensor is now limited by the input capacitive load of the electronic amplifier [5]. However, the X-Hall does not cope with the Flicker noise.

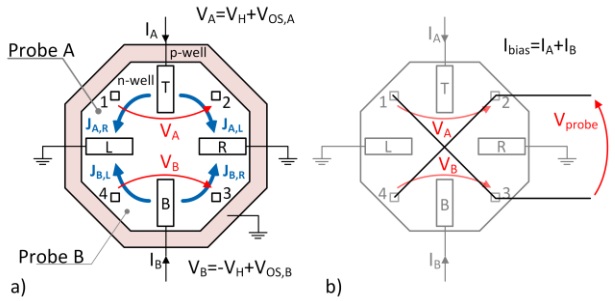

Fig. 2. a) Layout of the octagonal Hall-effect probe highlighting the bias connections. b) Scheme of the readout connections in the X-Hall architecture.

III. The Amplifier

The Hall-effect probe needs to be combined with a differential voltage amplifier that satisfies strict requirements: *i)* high-input impedance (megaohms) to absorb a theoretically zero current from the Hall-effect sensor; *ii)* closed-loop voltage gain greater than 50 as the Hall voltage is typically smaller than a few millivolts; *iii)* low residual offset voltage (smaller than a few microvolts). If we are also targeting wide bandwidth then the amplifier must also exhibit: *iv)* a minimum input capacitance (lower than 1 pF) and *v)* wide bandwidth (tens of MHz).

High-gain together with wide-bandwidth translates in gain-bandwidth-product (GBW) greater than 1 GHz, which is extremely challenging to achieve in power-CMOS technologies like the BCD. On the other hand, a power-CMOS technology is mandatory to get the high galvanic isolation between the sensed current and the sensor itself (e.g. 6-kV isolation in BCD6 technology). To cope with the gain-bandwidth requirement, we opted for a current-feedback amplifier (CFA), since this architecture does not stick to the constant GBW rule of voltage-feedback amplifiers and exploits low-impedance nodes to get wide bandwidth. The transistor-level scheme of the realized amplifier is reported in Fig. 4. The drawbacks of the CFA are high-offset and asymmetric inputs in terms of

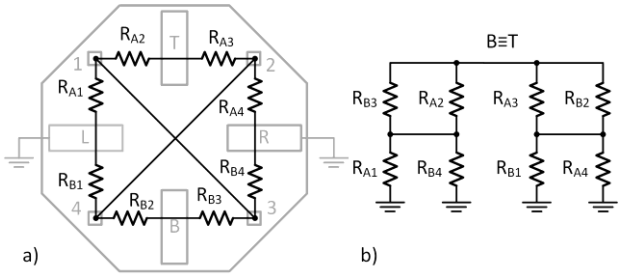

Fig. 3. Resistive bridge model of the XHall probe. a) Correspondence between each resistance and probe section. b) Common-centroid connection due to cross short circuiting.

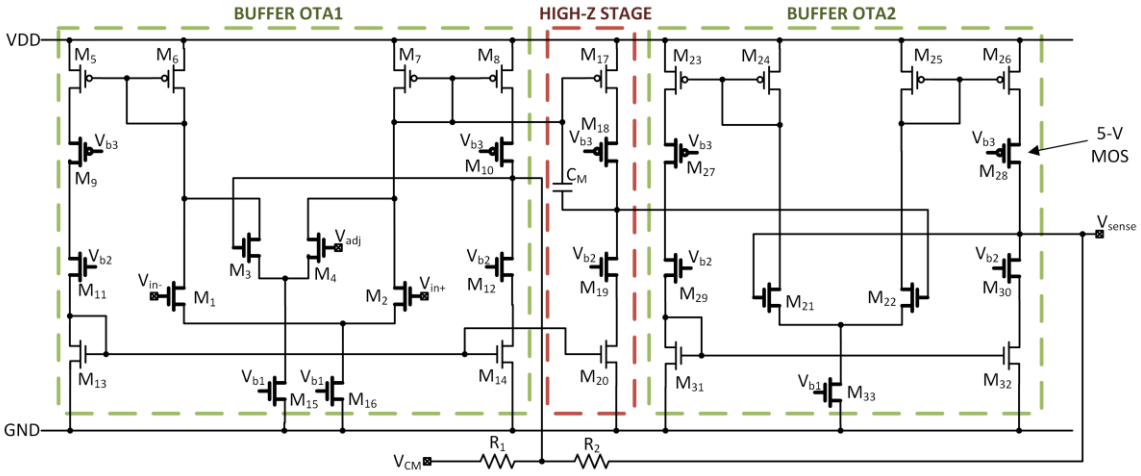

Fig. 4. Schematic diagram of the DDCFA highlighting the different types of MOSFETS.

input impedance. Offset issue is mitigated by designing the buffers of the CFA architecture as highly-symmetric, cascoded-output, single-stage, operational-transconductance amplifiers (OTA) in unity gain feedback. To amplify the differential output voltage V_{probe} of the Hall sensor without sinking an appreciable current, the OTA1 is a differential-difference amplifier (DDA) connected in instrumentation amplifier mode with the gain set to 1. This architecture of the OTA1 also provides an additional input (V_{adj}) to compensate for the offset of the CFA as well as the residual offset of the Hall sensor. Another important aspect of the OTA1 is the input capacitance that must be minimized without impinging on the open-loop gain of the OTA1 [6]. To this end, the two differential coupled pairs of the OTA1 are implemented by using 5-V graded MOSFETs with thick gate oxide and setting their size factor at the minimum value that allows achieving the target open-loop gain. On the contrary, all the current mirrors of both the OTAs are realized by using smaller 1.8-V graded MOSFETs to exploit their better dynamic performance and push the bandwidth of the whole amplifier to higher frequencies. Since the amplifier is 5-V supplied, all the 1.8-V MOSFETs are protected by cascoded 5-V MOSFETs that handle the high source-drain voltage drop. The gain stage of the CFA is realized by mirroring the output current of the OTA1 to a high-impedance node. A Miller capacitance is added for pole-zero cancellation. The OTA2 looks alike to OTA1 without differential-difference input.

All the transistors were sized to set the bandwidth above 50 MHz and minimize the total input-referred noise power, accounting for both Flicker noise and thermal noise. The CFA was optimized to work with a closed-loop gain of 35 dB given by resistive feedback with R_1 = 50 Ω and R_2 = 2 kΩ, and a maximum capacitive load at the output of 5 pF. The simulated GBW of the proposed DDCFA is 3.75 GHz with a load capacitance of 1 pF. An output stage with gain set to 2 is placed after the DDCFA to cope with external loads.

IV. Measurement Results

A prototype of the current sensor is implemented in 0.16-µm BCD8 technology provided by STMicroelectronics (Fig. 5). The silicon die is 4-mm^2 large but a single current sensor occupies approximately 1 mm^2 (the rest of the area is used for replica circuits and testing structures) and could be shrunk even more by optimizing the layout. Post-layout simulations of the complete current sensor report a typical current consumption of 5.5 mA (25 mW), which is in agreement with the state-of-the-art (Table II).

The sensitivity of the current sensor is given by the combination of the current-to-magnetic field transduction factor (approximately 2 mT/A from FEM simulations), the absolute sensitivity of the Hall probe, and the gain of the amplifier (100 from circuital simulations). They all are fixed gain factors apart from the sensitivity of the Hall-probe that is proportional to the bias current $I_{bias} = I_A + I_B$. Fig. 6-left reports the measured static characteristic of the current sensor for bias currents of 1 mA and 1.8 mA, reporting a total sensitivity of 23 mV/A (11.5 V/T) and 36 mV/A (18 V/T), respectively, which are comparable to the state of the art. The reference input current is generated by a controlled DC voltage supply applied across a known 1-Ω resistor. The input current used to make the static characteristic has been limited between -10 A and 10 A due to the testing setup but the current sensor can handle input currents as high as 20 A. The prototype shows a static linearity error of less than 1 % (inset of Fig. 6-left) that is good for the target applications. Noise performance is evaluated by means of the input-referred noise power spectrum density (PSD), which is shown in Fig. 6-center. The noise PSD shows an important Flicker noise component and a total rms noise of about 75 mA. The frequency response of the current sensor

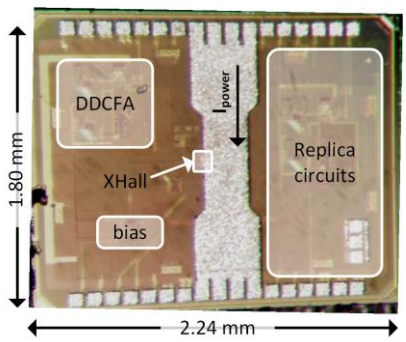

Fig. 5. Chip microphotograph.

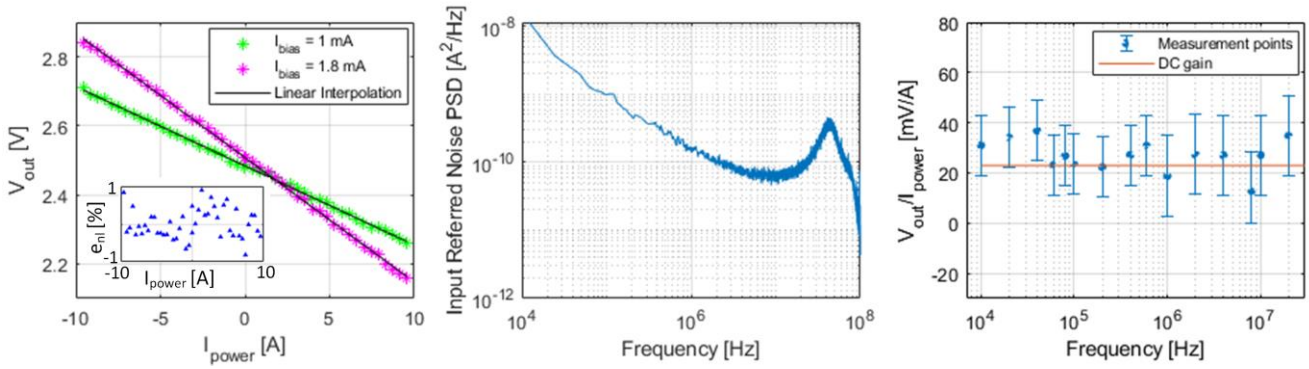

Fig. 6. left) Stetic characteristic of the current sensor for two different bias currents. Non-linearity error in the inset. center) Input-referred noise Power Spectrum Density computed at I_{bias} = 1 mA and showing a corner frequency at around 4 MHz. Noise peak at high frequencies is related to the second-order response of the DDCFA. right) Estimated transfer function up to 20 MHz after compensation for the inductive parasitic effect.

was preliminarily characterized by exciting the sensor with a pure sine-wave current input and performing FFT analysis on the output response of the sensor. The transfer function (TF) of the sensor was computed by dividing the output peak by the input sine wave amplitude and the estimated TF is shown in Fig. 6-right. Due to limitations in the available instrumentation, the amplitude of the exciting current sine wave was set to 100 mA, which is barely higher than the input-referred rms noise. This results in great variability in the estimation of each point of the TF. The prototype shows an unpredictable inductive parasitic effect that adds a coherent interference at the output of the current sensor. This interference was characterized and compensated by implementing a low-pass digital filter on the sensor output data. At higher frequencies, the parasitic element causes the saturation of the DDCFA and the TF cannot be correctly estimated. Though the parasitic effect limits the bandwidth of the prototype to 20 MHz (fig. 6-right) the sensor still overcomes the state of the art and can be used to record fast switching currents. Fig. 7 shows the fast transition (60 ns) of a 5-Vpp voltage (green line) across a 50-Ω resistor. The consequent current transition is recorded by using both a commercial 100-MHz current probe (red line) (Keysight N2783A) and our current sensor prototype (yellow line). The parasitic effects stress the overshoots in V_{OUT}, but the sensor is still able to detect the current edge with a delay comparable to that of the commercial probe.

Fig. 7. Detection of a 60-ns current edge.

TABLE II. STATE-OF-THE ART COMPARISON TABLE

	Sensor Type	Tech node [µm]	Area [mm²]	Bandwidth [MHz]	Input Range [A]	Supply [mA]	Sensitivity [mV/A]
[1]	Hall	0.35	/	1.7	300	4	/
[3]	Hall+ coil	0.18	3.17	75	±40	18.7	43.5
[5]	Hall	0.16	4	1	±10	4.4	42.5
THIS WORK	Hall	0.16	4	20	±20	5.5	36

V. CONCLUSION

The presented current sensor combines the X-Hall technique with a broadband DDCFA to enlarge the bandwidth of Hall-effect based current sensors. Though the realized prototype suffers from an inductive parasitic effect that limits the bandwidth, a 20-MHz bandwidth has been demonstrated, with the potentiality to be even wider. To our knowledge, this is the first Hall-effect probe that achieves a bandwidth higher than 3 MHz. Functionality of the sensor has been demonstrated in the detection of a fast current edge, but characterization of temperature dispersion must be still performed.

REFERENCES

[1] Y. Li, M. Motz, and L. Raghavan, "A Signal and Offset T&H Frontend for Spinning Hall Sensors with Ping-Pong and Chopping Techniques," in ESSCIRC 2018, 2018, pp. 338–341.

[2] L. Xu, J. H. Huijsing, and K. A. A. Makinwa, "A ±4A high-side current sensor with 25V input CM range and 0.9% gain error from −40°C to 85°C using an analog temperature compensation technique," in *2018 IEEE ISSCC*, 2018, pp. 324–326.

[3] T. Funk and B. Wicht, "A Fully Integrated DC to 75 MHz Current Sensing Circuit with On-Chip Rogowski Coil," in CICC, pp. 6–9, 2018.

[4] D. Bellasi, et al, "A Broadband Multi-Mode Compressive Sensing Current Sensor SoC in 0.16um CMOS," IEEE Trans. Circuits Syst. I Regul. Pap., vol. 66, no. 1, pp. 105–118, Jan. 2019.

[5] M. Crescentini, et al., "Bandwidth Limits in Hall Effect-based Current Sensors," Acta-IMEKO, vol. 6, no. 4, pp. 17–24, 2017.

[6] M. Crescentini, M. Marchesi, A. Romani, M. Tartagni, and P. A. Traverso, "A Broadband, On-Chip Sensor Based on Hall Effect for Current Measurements in Smart Power Circuits," IEEE Trans. Instrum. Meas., vol. 67, no. 6, pp. 1470–1485, 2018.

[7] M. Crescentini, M. Biondi, M. Marchesi, A. Romani, M. Tartagni, and P. A. Traverso, "Bandwidth enhancement in Hall probe by X-Hall DC biasing," J. Phys. Conf. Ser., vol. 1065, no. 5, Aug. 2018.